AIAA JOURNAL
Vol. 40, No. 10, October 2002

Energy-Dissipating Composite Members with Progressive Failure: Concept Development and Analytical Modeling

D. Stefan Dancila* and Erian A. Armanios†
Georgia Institute of Technology, Atlanta, Georgia 30332

A new concept for tailored, one-dimensional tensile composite members with sequential, progressive failure and yield-type response is presented. The concept is developed as a solution to a constrained arresting problem. Flexible composites, obtained by reinforcing an elastomeric matrix material with high-performance elastic fibers, are used to create a structure with redundant load paths and progressive failure. Three analytical models are developed for the prediction of response under stroke-controlled loading. The response of the tailored configuration is compared with that of conventional members of identical length, total cross-sectional area, and material properties. Analytical results confirm the predicted progressive failure sequence and yield-type response, as well as the increased energy-dissipation capability.

Nomenclature

A = cross-sectional area
a = acceleration
b = width
C = integration constants
E = normal elastic modulus
F = logical constant False; nondimensional force
K = overall equivalent spring stiffness
k = equivalent spring stiffness
L = overall length
l = segment length; connector length
m = mass
N = axial load
n = number of sublinks
P = tip axial load; permutation set
p = primary
q = shear lag parameter
S = Boolean vector
s = secondary; Boolean vector
T = logical constant True
t = thickness; terminal; time
u = displacement
V = velocity
x = Cartesian coordinate
β = material constant; length ratio
γ = thickness ratio
δ = displacement; arrest distance
ε = strain
λ = length ratio
μ = shear modulus
ν = amplitude parameter
ξ = nondimensional displacement
σ = stress
τ = shear stress
ϕ = failure-order permutation

Subscripts

c = connector
f = failure
p = primary; numerical index
q = numerical index
s = secondary

Superscripts

c = connector
p = primary
s = secondary
t = terminal
u = ultimate
$*$ = subdivided configuration

Introduction

COMPOSITE materials play an increasingly important role in structural applications. A large volume of published research work has established their potential as more than just lighter substitutes to conventional materials. Although representing a challenge for analysis, the anisotropic nature of composite material properties allows additional degrees of freedom for design. Tailoring of structural properties makes it possible to induce deformation modes that result in improved performance. An additional benefit, explored in the present work, is the ability to induce failure modes that result in improved energy dissipation as well.

For aerospace structures subjected to crash loading, it is generally accepted that the main design goal becomes that of crew/payload protection, typically represented by deceleration levels lower than maximal tolerable values and the preservation of a minimal crew/payload critical volume. Under such circumstances, structural integrity ceases to be a goal and may be difficult, or even impossible, to preserve. Structural failure modes that enhance crew/payload protection are considered desirable, and the design for and incorporation of such modes constitutes the object of crashworthiness efforts.

Although it is recognized that an optimal response to crashworthiness requirements is associated with a yield-type structural response, composite materials are generally characterized by a brittle behavior and, consequently, tend to dissipate less energy than their metallic counterparts. It is, therefore, desirable to increase the energy-dissipation capacity of composite materials. Crashworthiness research efforts have addressed this problem, and a number of composite structural concepts involving compressively loaded structures that crush under impulsive loading have been proposed and investigated.[1–7] Hamada and Ramakrishna[1] and Mamalis et al.[2] have investigated the compressive failure of composite tubular structures, whereas Knack and Vizzini[3] have focused their investigation on the energy absorbing capabilities of conical composite structures subject to off-axis loading. Jackson et al.[4] have investigated scaling laws applicable for energy absorption in composite plates, and

Received 23 February 2001; revision received 18 February 2002; accepted for publication 24 April 2002.

*Assistant Professor, School of Aerospace Engineering. Member AIAA.
†Professor, School of Aerospace Engineering. Associate Fellow AIAA.

Goldsmith and Sackman[5] have analyzed energy absorption in sandwich plates. The response of composite sine webs has been investigated by Hanagud et al.[6] with emphasis on the effect of a chamfer in the sine webs on the progression of failure and the energy-dissipation capacity of the structure. The energy-dissipating capacity of a subfloor beam structure has been investigated by Farley.[7] However, no investigations of the energy absorbing capabilities of composite structures subject to tensile loading have been reported in the literature.

With the goal of payload/crew protection in mind, it should, however, be recognized that the crew/payload support structure does not necessarily have to be subject to compressive loading as well. If, for example, one would conceive a support system in which ligament-type composite members are used to suspend the payload, such ligaments would be subject to tensile loading in the event of vertical crash impact, considered a representative condition for crashworthiness assessment. Motivated by this observation, the present work investigates the feasibility of composite members with yield-type response under tensile loading. A tailored composite material configuration is proposed and evaluated and is shown to be characterized by such a response, accomplished through the use of an elastomeric matrix, an internal redistribution of load, and a progressive failure of redundant load paths. The successful experimental validation of this tailoring concept and comparison with the analytically modeled response presented are the subject of a subsequent publication.

Development of Tailoring Concept

Consider a straight structural member with one end fixed and the opposite end arresting a moving body with mass m and velocity V, as shown in Fig. 1. It is required to arrest the body within constraints imposed on the deceleration level a, $0 \le a \le a_{\max}$, and on the distance δ over which the arrest is performed, $0 \le \delta \le \delta_{\max}$. As the member applies a restraint force to the moving body, kinetic energy is transformed into strain energy. If the member has an elastic response and preserves its integrity, at the point where the moving body is arrested the entire amount of kinetic energy has been converted into strain energy. Subsequently, under ideal conditions, if the strain energy is allowed to convert back into kinetic energy, the net effect is simply a reversal of direction for V. If, however, the structural member fails in the loading process, the kinetic energy converted up to that point into strain energy becomes unrecoverable, and the net effect is a reduction in the kinetic energy of the moving body. Ideally, should the failure of the structural member occur at the point where the body has zero velocity, a complete arrest could be achieved.

Figure 2 qualitatively illustrates the tip load P vs tip displacement δ linear response of a composite member for three cases. Also shown in Fig. 2 are the constraints of the problem, $\delta = \delta_{\max}$ and $P = P_{\max} = ma_{\max}$, and the area delimited by the constraints corresponds to the maximum amount of kinetic energy that can be converted while remaining within the bounds of the constraints. The curve labeled 1 corresponds to the case of a stiff member, for which the maximum acceleration constraint is met first. The curve labeled 2 corresponds to the case of a compliant member, for which the maximum displacement constraint is met first. Finally, the curve labeled 3 corresponds to the case where both constraints are met simultaneously. The amount of kinetic energy converted into strain energy of the composite member is largest in case 3. However, this value only represents 50% of the maximum attainable within the constraints.

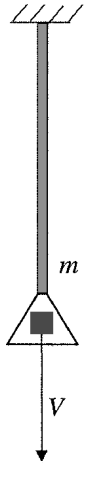

Fig. 1 Arrest using a structural member.

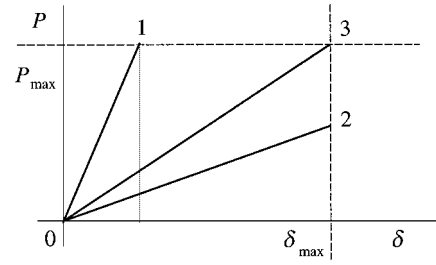

Fig. 2 Tip load vs displacement for a linear-response member.

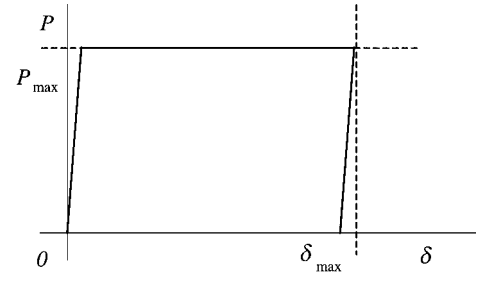

Fig. 3 Yield-type structural response.

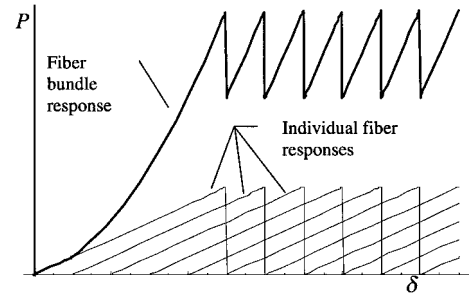

Fig. 4 Comparison of response for fiber vs fiber bundle.

A desirable response could be obtained by the use of a structural member with a nonlinear, yield-type, response. This response, qualitatively shown in Fig. 3, could be achieved by using a bundle of unidirectional fibers. The load-displacement curve for typical fibers is linear up to the point of failure. For an ideal bundle of equal length fibers connected at their ends, the load-displacement curve is also linear, with all fibers failing simultaneously. If, however, the bundle contains fibers with lengths tailored such that they have a uniform distribution over a specified length interval, there will be an offset between the points where individual fibers start carrying load. If, for example, the extreme length difference between fibers is larger than the ultimate fiber extension, failure of the shortest fiber will occur before the longest fiber starts carrying load.

The response of a tailored-length bundle is qualitatively shown in Fig. 4, where the superimposed triangles represent load-displacement curves of individual fibers, whereas the higher, jagged curve represents the load-displacement for the bundle, obtained as a summation of individual contributions of fibers. This load-displacement curve starts resembling the yield-type response identified as a desirable solution for the arresting problem. To ensure the dimensional stability of the fiber bundle and provide protection and load transfer, a bonding matrix material is needed. If a brittle matrix material such as epoxy is used, the tailored bundle of fibers will loose the desirable progressive failure response because all fibers will be loaded simultaneously. Moreover, in unidirectional brittle

matrix composites loaded along the fibers, the adjacent failure of a small number of fibers may trigger overall failure of the entire cross section. However, the use of an elastomeric material as a matrix for the bundle will preserve the fibers axial stiffness and strength while achieving a target level of bending compliance due to the reduced elastic moduli of the elastomeric matrix. This bending compliance characteristic is essential to the development of the technical solution proposed in the present work.

Consider the composite link, shown in Fig. 5, made of two segments of unequal length and connected at their ends. The two segments, referred to as primary and secondary, are made of the same material with modulus of elasticity E_{11} along their length direction. Their lengths, thickness, and cross-sectional areas are denoted by l_p and l_s, t_p and t_s, and A_p and A_s, respectively. Subscripts p and s denote primary and secondary quantities, respectively.

The following geometric choices are made for primary and secondary segments having the same width b:

$$t_p b = A_p < A_s = t_s b \tag{1}$$

When the fiber ultimate strain is denoted by ε_f^u, it is assumed that

$$(l_s - l_p) > 2l_p\varepsilon_f^u, \qquad (l_s - l_p) > l_p\varepsilon_f^u + l_s\varepsilon_f^u(A_p/A_s) \tag{2}$$

an assumption that serves to ensure the nonoverlapping of individual response curves in the development that follows, thereby allowing the benefits of the tailoring concept to become more apparent.

The lengths of the connector region l_c are assumed to be small:

$$l_c \ll l_p \tag{3}$$

The assumptions in Eqs. (2) and (3) are introduced for convenience at this stage of the development and will be relaxed later.

An axial stretching applied to the link connectors in Fig. 5 through applied load P leads to the load-displacement response shown schematically in Fig. 6. Because of the assumed difference in length between the two segments and their bending flexibility, an initial stage consists of load being developed solely by the primary segment. The load increases up to the point where the primary segment fails, at displacement $\delta_1 = l_p\varepsilon_f^u$ and load $P_1 = A_p E_{11}\varepsilon_f^u$. On failure of the primary segment, the load drops to 0, maintaining this value up to $\delta_2 = (l_s - l_p)$, where the secondary segment starts being stretched. Subsequently, the load increases up to the failure point of the secondary segment, which occurs at $\delta_3 = l_s - l_p + l_s\varepsilon_f^u$ and $P_3 = A_s E_{11}\varepsilon_f^u$. Based on the choices in Eq. (1), it follows that $P_3 > P_1$. The combined area under the two triangles in Fig. 6 represents the work of an external force P required to produce the complete failure of the link.

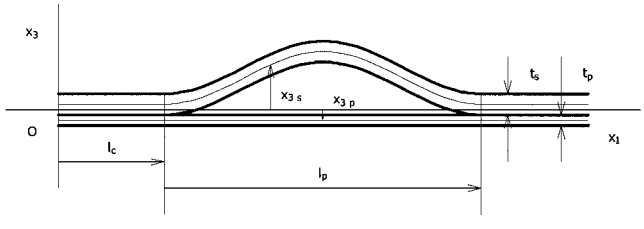

Fig. 5 Composite link.

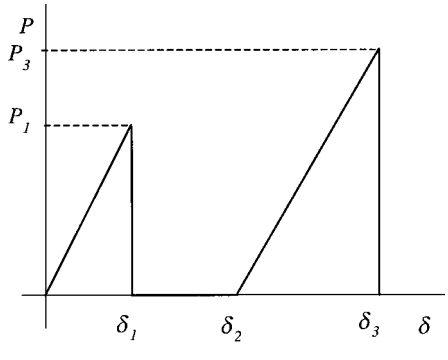

Fig. 6 Response of a composite link.

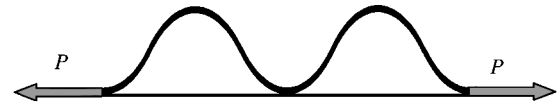

Fig. 7 Subdivided link.

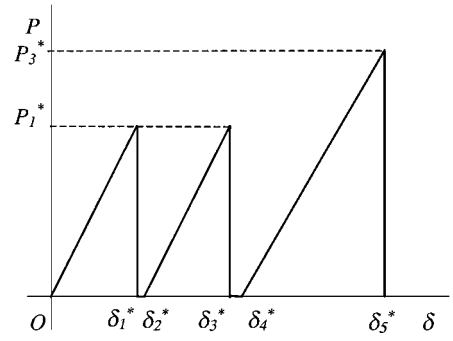

Fig. 8 Load vs displacement response of subdivided link.

If the link is subdivided in two equal sublinks by the introduction of an additional middle connector, as shown in Fig. 7, an increase in the area under the load-displacement curve will result, as depicted in Fig. 8. Load will be developed first by series connection of the two primary segments. At $P_1^* = A_p E_{11}\varepsilon_f^u$ and $\delta_1^* = l_p\varepsilon_f^u$, the primary segments are expected to fail. From the standpoint of an ideal model, the two segments should fail simultaneously. However, due to the statistical nature of failure loads, small differences can be assumed to exist, and one of the segments will fail first, causing the load in the member to drop to 0. On subsequent stretching being applied, at $\delta_2^* = (l_s - l_p)/2$ the system will start loading again. Based on Eq. (2), $\delta_2^* > \delta_1^*$. At this stage, the load path consists of the series combination of the remaining primary segment on one link and the secondary segment on the other link.

As a consequence of Eq. (1), the failure load of secondary segments is higher than that of primary ones. In a chaining of primary and secondary segments, the primary ones represent the weaker link. The failure of the remaining primary segment will occur at load $P_3^* = P_1^* = A_p E_{11}\varepsilon_f^u$ and displacement $\delta_3^* = (l_s - l_p)/2 + [l_p + l_s(A_p/A_s)]\varepsilon_f^u/2$, at which stage the load reduces to 0 again. Finally, continuing the stretching of the system, at $\delta_4^* = (l_s - l_p)$ the series combination of secondary segments starts loading. Failure of one secondary segment occurs at $\delta_5^* = (l_s - l_p) + l_s\varepsilon_f^u$ and $P_5^* = A_s E_{11}\varepsilon_f^u$. Based on Eq. (1), $P_5^* > P_1^* = P_3^*$.

The combined area under the three triangles in Fig. 8 represents the work of an external force P required to produce the complete failure of the link. When Figs. 6 and 8 are compared, the first and the third triangles are identical, whereas the middle one represents the benefit of the additional connector. This associated increase in energy dissipation is key to the development of the tailored composite concept.

Analytical Model

The single and double links shown in Figs. 5 and 7, respectively, could be extended to n sublinks as shown in the axonometric view of Fig. 9 for a tailored member with $n = 5$. With reference to the composite link in Fig. 5, the equations of the midplane surfaces for the primary and secondary layers are given by

$$0 \le x_1 \le L, \qquad 0 \le x_2 \le b, \qquad x_{3p} = -(t_s/2)$$

$$x_{3s} = \begin{cases} \dfrac{t_p}{2}, & i(l_c + l_p) \le x_1 \le i(l_c + l_p) + l_c, \qquad i = 0, n \\ \nu\dfrac{1 + \cos\{(2\pi/l_p)[x_1 - l_c - (l_p/2) - i(l_c + l_p)]\}}{2} & \\ \qquad i(l_c + l_p) + l_c \le x_1 \le (i+1)(l_c + l_p) + l_c & \\ \qquad\qquad i = 0, (n-1) \end{cases} \tag{4}$$

Fig. 9 Axonometric representation of a tailored composite member with $n = 5$.

The primary and secondary layers are made of unidirectional flexible composite material reinforced with continuous fibers oriented in the Ox_1x_3 plane of a Cartesian reference system $Ox_1x_2x_3$. Each link contains two subdomains, a connector domain and a segment domain. The connector domain, with a length l_c, has primary and secondary layers running parallel and bonded along the common interface. The segment domain, of length l_p, is characterized by a primary layer that remains flat, whereas the secondary layer assumes a haversine-type shape, as shown in Fig. 5.

The combined thickness of the composite member t is given by

$$t = t_p + t_s$$

and the overall length L is related to the other model parameters by

$$L = (n+1)l_c + nl_p$$

The secondary layer assumes a haversine-type shape. Its length can be computed as

$$l_s = \int_{l_c}^{l_p + l_c} \sqrt{1 + \frac{\nu^2\pi^2}{l_p^2}\sin^2\left[\frac{2\pi}{l_p}\left(x_1 - l_c - \frac{l_p}{2}\right)\right]}\,\mathrm{d}x_1 \qquad (5)$$

and if l_s is a prescribed parameter, Eq. (5) can be used to determine the value of the amplitude parameter ν.

Constitutive Equations for Flexible Composites

Flexible composites are defined in this paper as materials obtained by reinforcing an elastomeric matrix with long, parallel, elastic fibers. Based on whether the mechanical response of the elastomeric material is elastic or viscoelastic, the resultant flexible composite will have elastic, time-independent or viscoelastic, time-dependent properties.

The mechanical properties of fiber reinforced materials have been presented in the early works of Hashin and Rosen[8] and Hill[9] for the case of elastic constituent properties and circular fiber cross section. By the utilization of the correspondence principle, Hashin[10] and Schapery[11] later proposed extensions for the case of viscoelastic matrix. Zhao and Weng[12] have obtained the constitutive equations of a composite material consisting of an elastic matrix reinforced with aligned or randomly oriented elliptic cylinders. Li and Weng[13] extended the analysis to the case of viscoelastic matrix and elastic elliptic cylinders, also by utilizing the correspondence principle.

The assumed elliptical cross section of the fibers is intended to model the case where the reinforcement phase of the composite material is in the form of ribbons. This model is adopted in the present work. The constitutive equations were obtained by using Eshelby's[14] solution for an ellipsoidal inclusion and the Mori–Tanaka[15] mean-field theory. The results of this approach were verified in Ref. 13, for the limiting case of circular fibers, against the early results of Refs. 8 and 9 and were found to be accurate.

The constitutive equations for flexible composites are provided in Refs. 12 and 13 and could be evaluated for a wide range of material properties. However, for the particular range of constituent properties typical of flexible composites, some general conclusions can be drawn with respect to the two effective properties of interest for the present work: the longitudinal Young's modulus E_{11} and the longitudinal shear modulus μ_{12}.

Longitudinal Young's Modulus E_{11}

Numerical values of the constitutive equations of Refs. 12 and 13 evaluated for a typical flexible composite made of an E-glass-fiber/Sylgard 184 silicone system show that the response of the composite material to axial normal loading is practically rate independent, linearly elastic, and governed by the rule of mixtures for both elastic and viscoelastic matrix. Consequently, the response of the material to longitudinal axial loading is approximated in the remainder of this work by a simple linearly elastic model.

Longitudinal Shear Modulus μ_{12}

By contrast, the effective longitudinal shear modulus is not governed by the rule of mixtures. Its variation with fiber volume fraction is strongly nonlinear. For the range of constituent elastic properties of interest to the present work, μ_{12} remains on the order of μ_{matrix} for fiber volume fractions up to 0.6 and starts increasing rapidly for higher volume fractions.[15] For the case of a viscoelastic matrix, the response can be obtained from the elastic one by using the correspondence principle.

Analysis of Connector Load Transfer

Two aspects of particular relevance for the modeling of load transfer from one link to adjacent ones through a connector are addressed for each connector load configuration: the interfacial shear stress distribution and the equivalent connector spring stiffness. When the tailored composite configuration shown in Figs. 5 and 9 and its associated failure sequence are considered, it can be recognized that, depending on the failure stage of adjacent links, a connector can be subject to five loading configurations.

The primary–primary (P–P) loading configuration, shown in Fig. 10a, corresponds to the case where neither one of the adjacent links experienced a failure of their respective primary segments. Consequently, the connector is subject to loading applied through primary segments at both ends. The thick horizontal lines in Fig. 10a represent unbonded interfaces between primary and secondary segments in the regions extending beyond connector ends. The primary–secondary (P–S) loading, shown in Fig. 10b, corresponds to the case where one of the adjacent links did experience a failure of its primary segment. The connector is subject to loading applied through the primary segments at one end and through the secondary segment at the other end. The secondary–secondary (S–S) loading, shown in Fig. 10c, corresponds to the stage at which both adjacent links experienced a failure of their respective primary segments. Consequently, the connector is subject to loading applied through secondary segments at both ends. The terminal–primary (T–P) loading, shown in Fig. 10d, corresponds to an end connector subject to loading applied through the adjacent primary segment. Finally, the terminal–secondary (T–S) loading, shown in Fig. 10e, corresponds to an end connector subject to loading applied through the adjacent secondary segment.

The stress and strain distributions in a connector subject to the loading configurations in Fig. 10 are obtained using a shear lag model.

Connector Stress Analysis

Consider an infinitesimal connector element of length dx_1, as shown in Fig. 11, where u_p and u_s represent the midplane displacements of the primary and secondary layers, respectively. Denoting the normal stress components in the x_1 direction in the primary and secondary layers by σ_p and σ_s, respectively, one can write

$$\sigma_s = E_{11}\frac{\mathrm{d}u_s}{\mathrm{d}x_1}, \qquad \sigma_p = E_{11}\frac{\mathrm{d}u_p}{\mathrm{d}x_1} \qquad (6)$$

The interfacial shear stress component τ can be computed as

$$\tau = \mu_{12}\frac{2(u_s - u_p)}{(t_s + t_p)} \qquad (7)$$

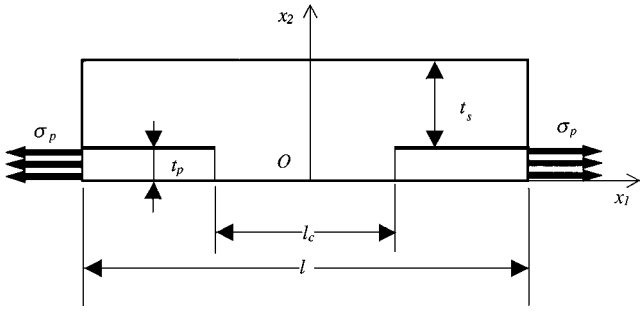

a) P–P connector loading configuration

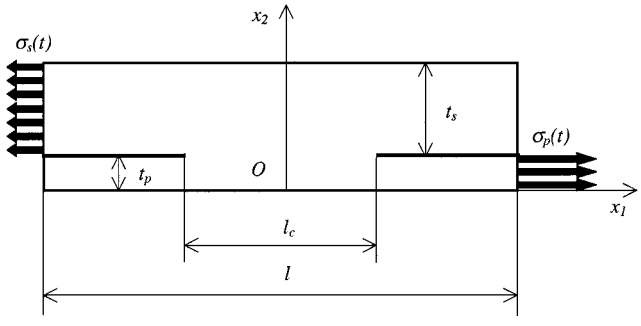

b) P–S connector loading configuration

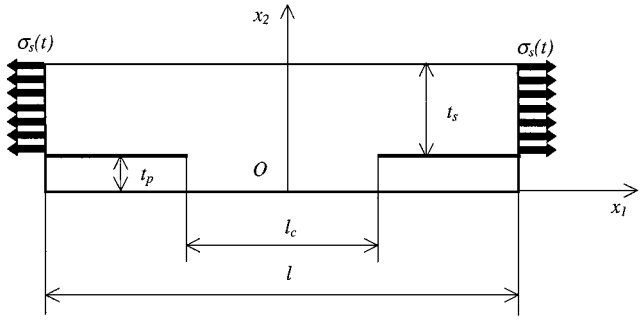

c) S–S connector loading configuration

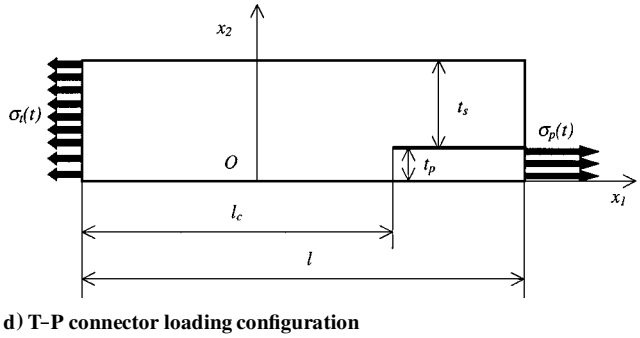

d) T–P connector loading configuration

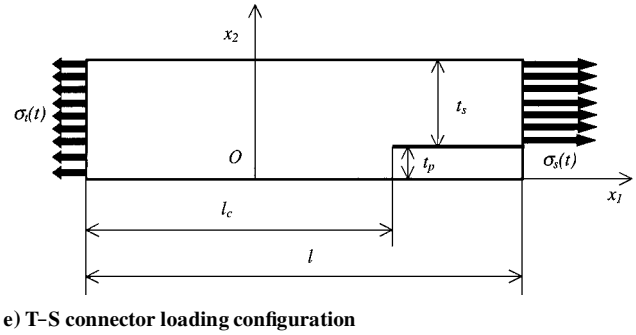

e) T–S connector loading configuration

Fig. 10 Connector loading configurations.

Table 1 Basic configuration parameter values

Property	Value
E_{11}	58.01 GPa
μ_{12}	5.24 MPa
ε_f^u	0.04
n	10
t_p	1.524×10^{-4} m
t_s	3.048×10^{-4} m
l_p	38.1×10^{-3} m
l_s	45.7×10^{-3} m
l_c	38.1×10^{-3} m
b	25.4×10^{-3} m

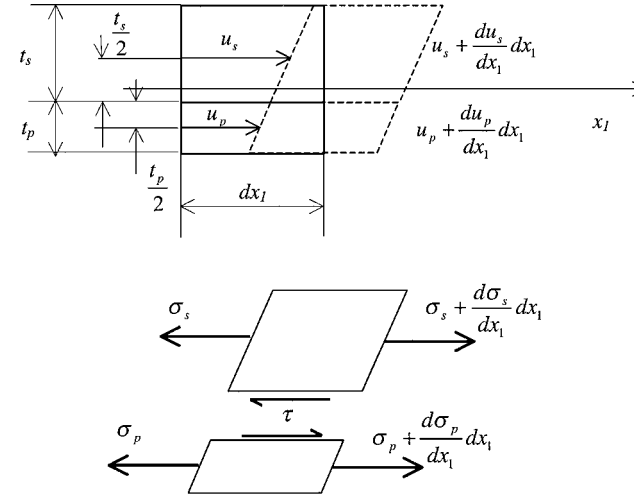

Fig. 11 Connector infinitesimal element.

The equilibrium equations for the two infinitesimal layer elements become

$$E_{11} t_s \frac{\mathrm{d}^2 u_s}{\mathrm{d}x_1^2} - 2\mu_{12} \frac{(u_s - u_p)}{(t_s + t_p)} = 0$$

$$E_{11} t_p \frac{\mathrm{d}^2 u_p}{\mathrm{d}x_1^2} + 2\mu_{12} \frac{(u_s - u_p)}{(t_s + t_p)} = 0$$

for which the general solution can be expressed as

$$\begin{aligned} u_s(x_1) = {} & [1/2q(t_p + t_s)]\{(C_3 - C_4)e^{-qx_1}(e^{2qx_1} - 1)t_p \\ & + q[2t_s(C_1 + C_3 x_1) + t_p(2C_2 + C_1 e^{-qx_1} - C_2 e^{-qx_1} \\ & + C_1 e^{qx_1} - C_2 e^{qx_1} + 2C_4 x_1)]\} \\ u_p(x_1) = {} & [1/2q(t_p + t_s)]\{-(C_3 - C_4)e^{-qx_1}(e^{2qx_1} - 1)t_s \\ & + q[2t_p(C_2 + C_4 x_1) + t_s(2C_1 - C_1 e^{-qx_1} + C_2 e^{-qx_1} \\ & - C_1 e^{qx_1} + C_2 e^{qx_1} + 2C_3 x_1)]\} \end{aligned} \tag{8}$$

where

$$q = \sqrt{2\mu_{12}/E_{11} t_p t_s} \tag{9}$$

The integration constants C_1, C_2, C_3, and C_4 are determined from the imposed boundary conditions corresponding to the five loading configurations. The shear stress distribution is obtained by using Eqs. (7–9), and the equivalent connector spring stiffness is computed as the ratio of applied load to overall extension.

The shear stress values are normalized with respect to an equivalent average shear stress $\tau = N_{x_1}/bl_c$, where N_{x_1} represents the total axial force applied. The coordinate x_1 is normalized with respect to l_c. The shear stress distribution and equivalent spring stiffness for the five loading configurations shown in Fig. 10 are given by

$$\tau_c^{pp}(x_1) = -\mu_{12}\frac{2\exp[q(l_c-2x_1)/2][\exp(2qx_1)-1]N_{x_1}}{b[1+\exp(ql_c)]E_{11}qt_p(t_p+t_s)}, \qquad k_c^{pp} = \frac{b(1+e^{ql_c})E_{11}qt_p(t_p+t_s)}{(1+e^{ql_c})l_cqt_p+2(-1+e^{ql_c})t_s}$$

$$\tau_c^{ps}(x_1) = -\mu_{12}\frac{2\exp[q(l_c-2x_1)/2](\{1+\exp[q(l_c+2x_1)]\}t_p+[\exp(ql_c)+\exp(2qx_1)]t_s)N_{x_1}}{b[-1+\exp(2ql_c)]E_{11}qt_pt_s(t_p+t_s)}$$

$$k_c^{ps} = \frac{b(-1+e^{2ql_c})E_{11}qt_pt_s(t_p+t_s)}{\left[(1+e^{2ql_c})t_p^2+(4e^{ql_c}+(-1+e^{2ql_c})l_cq)t_pt_s+(1+e^{2ql_c})t_s^2\right]}, \qquad \tau_c^{ss}(x_1) = \mu_{12}\frac{2\exp[q(l_c-2x_1)/2][\exp(2qx_1)-1]N_{x_1}}{b[1+\exp(ql_c)]E_{11}qt_p(t_p+t_s)}$$

$$k_c^{ss} = \frac{b(1+e^{ql_c})E_{11}qt_s(t_p+t_s)}{(1+e^{ql_c})l_cqt_s+2(-1+e^{ql_c})t_p}, \qquad \tau_c^{tp}(x_1) = -\mu_{12}\frac{2\exp[q(l_c-2x_1)/2]\{\exp[q(l_c+2x_1)]-1\}N_{x_1}}{b[1+\exp(2ql_c)]E_{11}qt_p(t_p+t_s)}$$

$$k_c^{tp} = \frac{b(1+e^{2ql_c})E_{11}qt_p(t_p+t_s)}{(1+e^{2ql_c})l_cqt_p+(-1+e^{2ql_c})t_s}, \qquad \tau_c^{ts}(x_1) = \mu_{12}\frac{2\exp[q(l_c-2x_1)/2]\{\exp[q(l_c+2x_1)]-1\}N_{x_1}}{b[1+\exp(2ql_c)]E_{11}qt_s(t_p+t_s)}$$

$$k_c^{ts} = \frac{b(1+e^{2ql_c})E_{11}qt_s(t_p+t_s)}{(1+e^{2ql_c})l_cqt_s+(-1+e^{2ql_c})t_p} \tag{10}$$

A comparison of connector interfacial shear stress distributions for the five loading configuration is provided in Ref. 16. For illustration purposes, a connector configuration is assumed, characterized by the parameter values listed in Table 1. Numerical values for the equivalent spring stiffness for all five connector loading configurations, normalized by equivalent connector stiffness $k = E_{11}bt/l_c$, are provided in Table 2.

Although the analysis was performed for the elastic response case, the extension to viscoelastic response by using the correspondence principle is straightforward.

Failure Prediction

The stress and strain distributions in the primary, secondary, and connector segments are the basis for predicting the tailored progression of failure. With respect to the primary and secondary segments, a tensile load applied at the ends of the tailored composite structure is transmitted to each composite link and results in a normal stress loading of the active segment, given by

$$\sigma_p = N_{x_1}\big/bt_p \tag{11}$$

if the primary segment did not fail or

$$\sigma_s = N_{x_1}\big/bt_s \tag{12}$$

otherwise where N_{x_1} represents the axial load applied.

The interfacial shear stress in the connector region is provided in Eq. (10) for the different loading configurations. The distribution of normal stresses in the primary and secondary layers over the connector domain can be also obtained from the displacements u_p and u_s by using Eq. (6). Consistent with the shear lag joint model adopted, the state of stress is then a superposition of these two stress states.

A simple, noninteracting, mixed failure criterion, applicable in the case of normal and shear loading along the fibers direction, is adopted in the present work. This criterion can be expressed as

$$\varepsilon_{11} \le \varepsilon_f^u, \qquad \tau_{12} \le \tau_{\max} \tag{13}$$

where ε_f^u represents the ultimate strain of the fibers and $\tau_{\max}$ a maximum longitudinal shear stress.

A similar criterion can be postulated for the case of viscoelastic matrix by retaining the first of Eq. (13) and replacing the second one with the criterion proposed by Laheru[17] for viscoelastic matrix composites loaded in longitudinal shear, resulting in

$$\varepsilon_{11} \le \varepsilon_f^u, \qquad \bar{t}/\bar{t}_0 = \left(\tau_{12}\big/\tau_{12}^0\right)^\beta \tag{14}$$

where $\bar{t}$ denotes time to failure under the shearing stress τ_{12}, $\bar{t}_0$ denotes time to failure under a shearing stress τ_{12}^0, and β is a material constant. Reference 16 contains the derivation of the second Eq. (14) based on Miner's linear cumulative damage hypothesis and shows the criterion to be in good agreement with experimental results for the failure of a fiberglass/rubber bonded system.

Based on Eq. (6) and Eqs. (11–14), the failure axial load for primary and secondary segments, denoted by P_p and P_s, respectively, can be expressed as

$$P_p = E_{11}bt_p\varepsilon_f^u, \qquad P_s = E_{11}bt_s\varepsilon_f^u \tag{15}$$

for both elastic and viscoelastic matrix response.

Determination of Connector Length

The connector failure mode is an interfacial debonding due to shear stress loading. With all other model parameters fixed, the design goal becomes the determination of connector length l_c that prevents connector failure. Whereas the response of elastic materials depends on the instantaneous loading applied, the response of viscoelastic ones depends on the entire loading history. Consequently, the two cases are to be treated separately in the sequel.

Elastic Matrix Material

The connector interfacial shear stress distributions, Eq. (10) for the different loading configurations, shows that loading configuration P–S, subject to axial force P_p, represents the critical condition for connector design. Consequently, the connector length can be determined from the inequality

$$\left|\mu_{12}\frac{2\exp[q(l_c-2x_1)/2](\{1+\exp[q(l_c+2x_1)]\}t_p+[\exp(ql_c)+\exp(2qx_1)])t_s]P_p}{b[-1+\exp(2ql_c)]E_{11}qt_pt_s(t_p+t_s)}\right| \le \tau_{\max}, \qquad x_1 \in \left[-\frac{l_c}{2},\frac{l_c}{2}\right] \tag{16}$$

Table 2 Normalized equivalent connector stiffness

Configuration	k_c/k
P–P	0.417
P–S	0.449
S–S	0.741
T–P	0.547
T–S	0.829

Viscoelastic Matrix Material

Because the response in this case is dependent on the loading history, as well as the failure sequence of individual links, which is stochastic in nature, a general closed-form solution is intractable. One could assume a conservative loading history given by the maximal load during the progressive failure sequence P_p applied over a period that exceeds the expected response time. Considering the application of such a load history as a worst-case scenario, one could attempt to obtain a conservative value for the connector length by

using the solutions for the elastic case in conjunction with the correspondence principle.

Response Modeling for Tailored Composite Member

The failure of the tailored composite member is characterized by a sequential, progressive failure of n primary segments, followed by the failure of one secondary segment. The order of failure is governed by the statistical distribution of failure loads among the primary segments and the secondary ones, respectively. The failure sequence determines the load redistribution within the tailored member during the $(n+1)$ response stages. During each such stage, each given connector is subject to one of the five loading configurations, shown in Fig. 10, depending on connector location and status of adjacent primary segments.

The response of tailored composite members subject to a stroke-controlled loading is modeled by using a chain-of-springs analogy. Three models, capturing the response of the tailored member to varying degrees of accuracy, are developed.

Accurate-Connector Stiffness Model

This analytical model accounts for the change in connector stiffness due to failure sequence and load redistribution. Because the failure sequence is stochastic, the model inherits this characteristic as well.

Define the equivalent spring stiffnesses for primary and secondary segments by

$$k_p = E_{11} b t_p / l_p, \qquad k_s = E_{11} b t_s / l_s \tag{17}$$

Let P_n represent the set of all permutations of the sequence $\{1, 2, 3, \ldots, n\}$, with card $(P_n) = n!$, and let $\varphi \in P_n$ be a randomly chosen member of this permutations set, interpreted as the failure sequence of the n links. Let s be an n-dimensional Boolean vector, the components of which are interpreted as current status of the n links. Initially,

$$s_i = T, \qquad (\forall) i \in \overline{1, n}$$

where T represents the Boolean value True and is interpreted as unfailed link state while F represents the Boolean value False and is interpreted as failed link state.

Provided that at the end of every computational stage i, $1 \le i \le n$, a link status update is performed by $s_j = F$ where $j = \varphi_i$, the set of equivalent stiffness of the tailored composite member can be consecutively computed by

$$K_i = 1 \Bigg/ \left(\sum_{p=1}^{n+1} \frac{1}{k_c^p} + \sum_{q=1}^{n} \frac{1}{k_l^q} \right), \qquad 1 \le i \le (n+1) \tag{18}$$

where

$$k_c^p = \begin{cases} k_c^{tp} & ((p=1) \wedge \neg s_1) \vee ((p=(n+1)) \wedge \neg s_n) \\ k_c^{ts} & ((p=1) \wedge s_1) \vee ((p=(n+1)) \wedge s_n) \\ k_c^{pp} & (2 \le p \le n) \wedge s_{p-1} \wedge s_p \\ k_c^{ps} & (2 \le p \le n) \wedge (s_{p-1} \forall s_p) \\ k_c^{ss} & (2 \le p \le n) \wedge \neg s_{p-1} \wedge \neg s_p \end{cases}$$

represents the equivalent stiffness of connector p and

$$k_l^q = \begin{cases} k_p & s_q \\ k_s & \neg s_q \end{cases}$$

represents the equivalent segment stiffness of link q.

The load developed by the tailored member as a function of end displacement δ can be expressed as

$$P(\delta) = \sum_{i=1}^{n+1} P_i(\delta) \tag{19}$$

where

$$P_i = \begin{cases} K_i(\delta - (i-1)(l_s - l_p)) & \delta \in \left(\delta_i^s, \delta_i^u\right], \\ 0, & \delta \notin \left(\delta_i^s, \delta_i^u\right], \end{cases} \quad 1 \le i \le (n+1) \tag{20}$$

$$\delta_i^s = \begin{cases} 0, & i = 1 \\ \max\left[\delta_{i-1}^u, (i-1)(l_s - l_p)\right], & 1 < i \le (n+1) \end{cases} \tag{21}$$

represents the end displacement at which the structure with $i-1$ primary failed links starts carrying load, whereas

$$\delta_i^u = \begin{cases} (i-1)(l_s - l_p) + (P_p/K_i), & i \ne (n+1) \\ (i-1)(l_s - l_p) + (P_s/K_i), & i = (n+1) \end{cases} \tag{22}$$

represents the end displacement at which the ith failure occurs.

A nondimensional form of load and tip displacement is given by

$$F = P / E_{11} b (t_p + t_s) \varepsilon_f^u \tag{23}$$

$$\xi = \delta \big/ L \varepsilon_f^u \tag{24}$$

The quantities used as reference in the normalization process represent the load and tip displacement, respectively, of a conventional composite member with identical overall length, total cross-sectional area, and material properties.

The response of the model developed is governed by 10 parameters, divided into two groups: material property parameters and geometric parameters. The first group consists of the longitudinal axial modulus E_{11}, the longitudinal shear modulus μ_{12}, and the fiber failure strain ε_f^u. The second group consists of the number of links n, the length of the primary segments l_p, the length of secondary segments l_s, the connector length l_c, the thickness of the primary layer t_p, the thickness of the secondary layer t_s, and the width b.

A base configuration is defined and used to illustrate the response predictions of the models. The parameter values defining this configuration are given in Table 1. The response of the model is shown in Fig. 12 for the parameter values indicated and an assumed failure sequence defined by the randomly chosen permutation $\varphi = \{1, 10, 6, 7, 9, 8, 3, 4, 5, 2\}$. For comparison purposes, Fig. 12 includes the response of a conventional composite member with the same length, total cross-sectional area, and material properties. Figure 12 illustrates the sequence of 10 primary segment failures, followed by the failure of a secondary segment. Also note that the response approximates a yield-type behavior.

Averaged-Connector Stiffness Model

This model represents a simplified version of the first, obtained by assuming an averaged equivalent spring stiffness for the connectors. Consequently, the model becomes insensitive to failure sequence and becomes deterministic.

Based on the results in Table 1, an average value of 0.536 is assumed for the normalized connector stiffness. The connector stiffness can then be expressed by

$$k_c = 0.536[E_{11} b (t_p + t_s)/l_c]$$

This constant value of connector stiffness simplifies Eq. (18), which reduces to

$$K_i = \frac{k_p k_s k_c}{(n-i+1)k_s k_c + (i-1)k_p k_c + (n+1)k_p k_s} \tag{25}$$

With K_i given by Eq. (25), Eqs. (19–22) are used to obtain the model response, which is nondimensionalized by using Eqs. (24) and (25). Out of the 10 controlling parameters, only 9 are explicitly controlling the present model. The effect of the other parameter, μ_{12}, is embedded in the constant used as an average value for the normalized connector stiffness. Algebraic manipulations reveal that the nine remaining parameters can be recast into a set of five nondimensional and four dimensional parameters. The five nondimensional parameters control the shape of the nondimensional response. All parameters control the scaling of the nondimensional response to

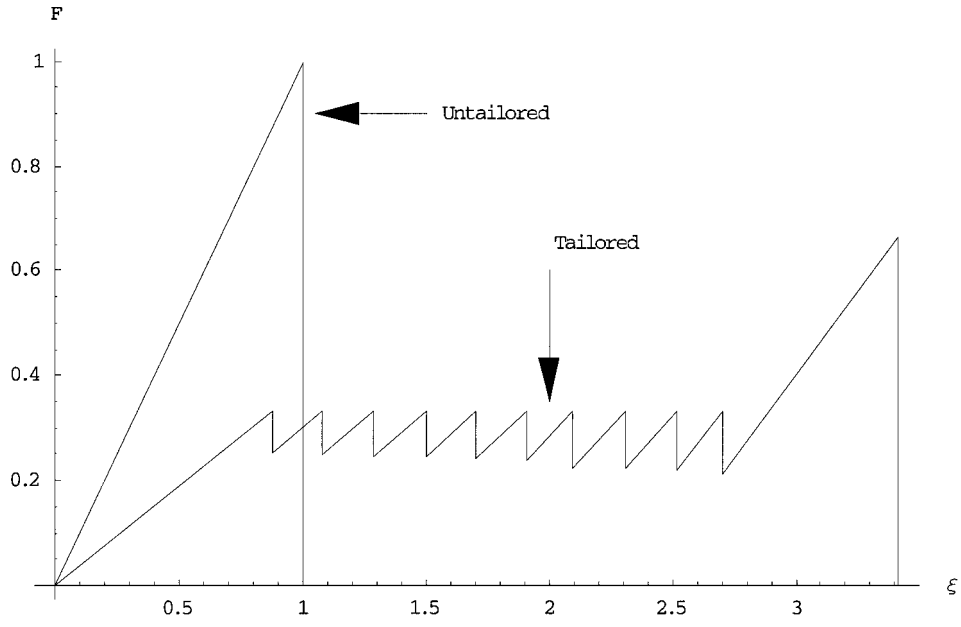

Fig. 12 Accurate-connector stiffness model nondimensionalized response of tailored member, $n = 10$.

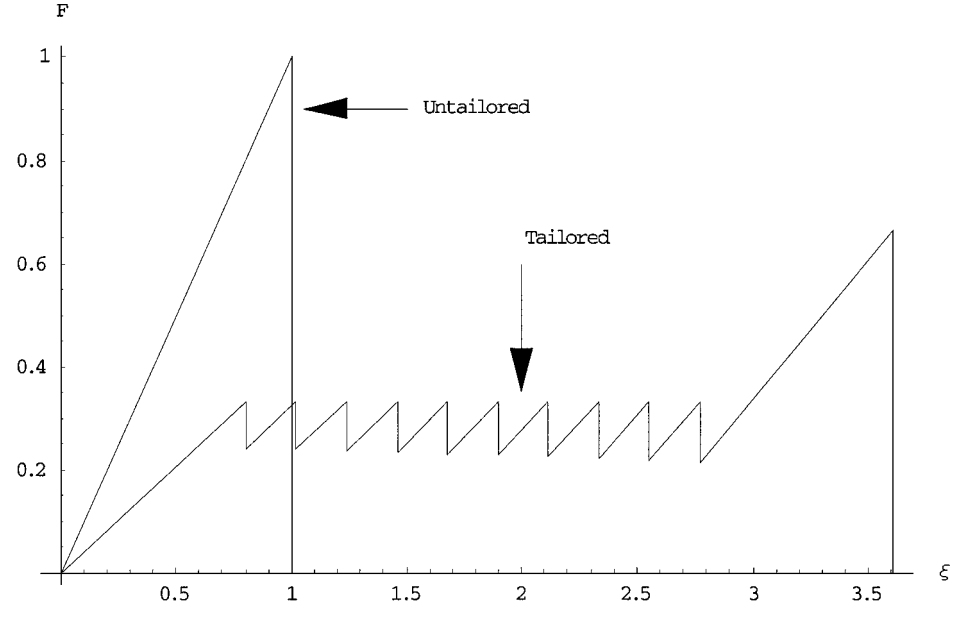

Fig. 13 Average-connector stiffness model nondimensionalized response of tailored member, $n = 10$.

the physical domain. Three of the nondimensional parameters are defined by

$$\gamma = t_s/t_p, \qquad \lambda = l_s/l_p, \qquad \beta = l_c/l_p \tag{26}$$

and the remaining two are ε_f^u and n.

When the same basic configuration tailored composite member is considered, the response prediction of the present model is shown in Fig. 13.

Negligible-Connector Model

The simplest analytical model for the tailored composite member that still captures the essential elements of the response can be developed based on the simplifying assumption $l_c \ll l_p$. This assumption represents the limiting case of either large l_p values, corresponding to long members subdivided in few links by short connectors or very small l_c values, made possible by high μ_{12} values.

Based on this assumption, the connector is reduced to a point at which adjacent links connect and transfer load. The equivalent spring stiffness of this model can be expressed as

$$K_i = \frac{k_p k_s}{(n-i+1)k_s + (i-1)k_p} \tag{27}$$

As one other parameter, l_c, ceases to influence the response, its corresponding nondimensional counterpart, β in Eq. (26), is dropped, and the eight remaining parameters are recast into a set of four nondimensional and four dimensional parameters as before. Although all parameters control the scaling of the nondimensional response to the physical domain, only the four nondimensional parameters control the shape of the nondimensional response of the model. Figure 14 shows the response predictions of this simplified model for the basic tailored composite configuration considered.

Figure 12 shows that the development model captures the yield-type behavior of the tailored composite member and provides its characteristic progressive failure sequence. The approximations associated with each connector-stiffness model are reflected in the predicted tip displacement of the tailored member. According to the nondimensionlized force-displacement response in Figs. 12–14, for the particular choice of tailoring parameters presented, the negligible-connector model results in a tip displacement that is about

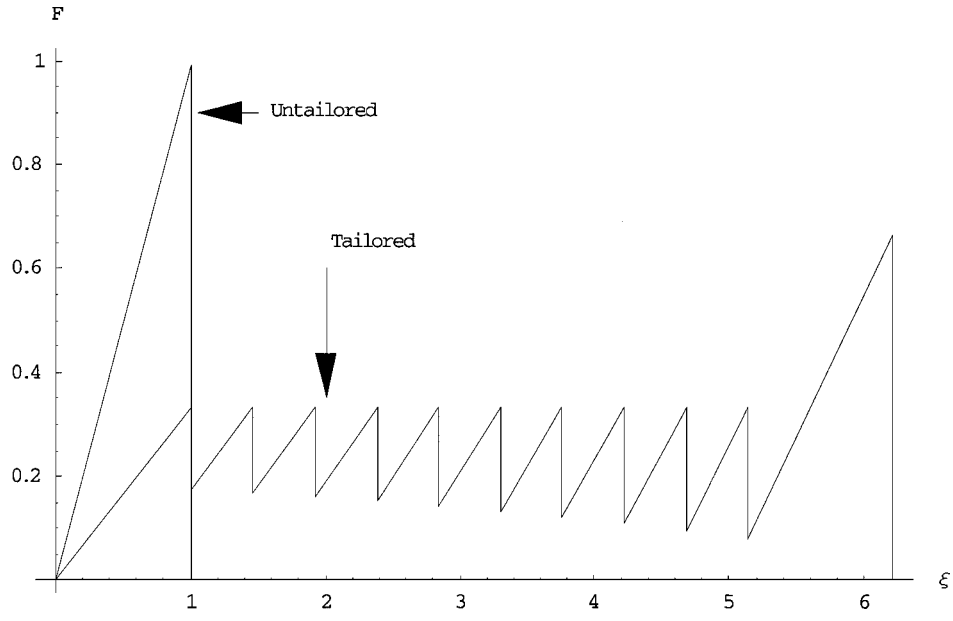

Fig. 14 Negligible-connector model nondimensionalized response of tailored member, $n = 10$.

six times that of the conventional member, whereas this value drops to about three times for the average and accurate-connector stiffness models. For this choice of tailoring parameters, all models indicate a reduction of about 33% in maximum force. Comparison of areas under the nondimensionlized force-displacement curves shows for these cases a 207, 111, and 96% increase relative to the conventional member, for the negligible-, average-, and accurate-connector stiffness models, respectively. This increase illustrates the gain in energy dissipation achieved by the tailored composite member. However, these values do not represent the maximal capabilities of the tailoring concept and only reflect the response of a tailoring configuration used in the experimental verification phase and selected here for the purpose of illustration of typical response.

Conclusions

A new concept for tailored one-dimensional tensile composite members with sequential, progressive failure, and yield-type response was presented. This tailored progression failure behavior is achieved by using a flexible composite system made of high-performance elastic fibers embedded in an elastomeric matrix. Three analytical models are developed for the prediction of response under stroke-control loading, and the parameters controlling the response are isolated. Results confirm the yield-type response achieved by the tailored composite member, its sequential progressive failure, and the associated increase in energy-dissipation measure compared to a conventional member of identical length, cross-sectional area, and material properties. The successful experimental validation of this tailoring concept and comparison with the analytically modeled response presented are the subject of a subsequent publication.

Acknowledgment

The authors would like to acknowledge the Georgia Space Grant Consortium for its support.

References

[1]Hamada, H., and Ramakrishna, S., "Scaling Effects in the Energy Absorption of Carbon-Fiber/PEEK Composite Tubes," *Composites Science and Technology*, Vol. 55, No. 3, 1995, pp. 211–221.

[2]Mamalis, A. G., Yuan, Y. B., and Viegelahn, G. L., "Collapse of Thin-Wall Composite Sections Subjected to High Speed Axial Loading," *International Journal of Vehicle Design*, Vol. 13, No. 5–6, 1992, pp. 564–579.

[3]Knack, J. L., and Vizzini, A. J., "Energy Absorption of Truncated Kevlar Epoxy Cones Under Side Loads," *Proceedings of the 35th AIAA/ASME/ASCE/AHS/ASC Structures, Structural Dynamics, and Materials Conference*, Pt. 5, AIAA, Washington, DC, 1994, pp. 2831–2837.

[4]Jackson, K. E., Morton, J., Lavoie, J. A., and Boitnott, R., "Scaling of Energy Absorbing Composite Plates," *Journal of the American Helicopter Society*, Vol. 39, No. 1, 1994, pp. 17–23.

[5]Goldsmith, W., and Sackman, J. L., "Energy Absorption by Sandwich Plates. A Topic in Crashworthiness," *Crashworthiness and Occupant Protection in Transportation Systems—1991*, Applied Mechanics Div., Vol. 126, American Society of Mechanical Engineers, 1991, New York, pp. 1–30.

[6]Hanagud, S., Craig, J. I., Sriram, P., and Zhou, W., "Energy Absorption Behavior of Graphite Epoxy Composite Sine Webs," *Journal of Composite Materials*, Vol. 23, No. 5, 1989, pp. 448–459.

[7]Farley, G. L., "Crash Energy Absorbing Subfloor Beam Structure," *Journal of the American Helicopter Society*, Vol. 32, No. 4, 1987, pp. 28–38.

[8]Hashin, Z., and Rosen, B. W., "The Elastic Moduli of Fiber Reinforced Materials," *Journal of Applied Mechanics*, Vol. 31, No. 2, 1964, pp. 223–232.

[9]Hill, R., "Elastic Properties of Reinforced Solids: Some Theoretical Principles," *Journal of the Mechanics and Physics of Solids*, Vol. 11, No. 5, 1963, pp. 357–372.

[10]Hashin, Z., "Viscoelastic Fiber Reinforced Materials," *AIAA Journal*, Vol. 4, No. 8, 1966, pp. 1411–1417.

[11]Schapery, R. A., "Stress Analysis of Viscoelastic Composite Materials," *Journal of Composite Materials*, Vol. 1, No. 3, 1967, pp. 228–267.

[12]Zhao, Y. H., and Weng, G. J., "Effective Elastic Moduli of Ribbon-Reinforced Composites," *Journal of Applied Mechanics*, Vol. 57, No. 1, 1990, pp. 158–167.

[13]Li, J., and Weng, G. J., "Stress–Strain Relations of a Viscoelastic Composite Reinforced with Elliptic Cylinders," *Journal of Thermoplastic Composite Materials*, Vol. 10, No. 1, 1997, pp. 19–30.

[14]Eshelby, J. D., "The Determination of the Elastic Field of an Ellipsoidal Inclusion, and Related Problems," *Proceedings of the Royal Society of London*, Vol. A241, No. 1226, 1957, pp. 376–396.

[15]Mori, T., and Tanaka, K., "Average Elastic Stress in the Matrix and Average Elastic Energy of Materials with Misfitting Inclusions," *Acta Metallurgica*, Vol. 21, No. 15, 1973, pp. 571–574.

[16]Dancila, D. S., "Energy-Dissipating Composite Members with Progressive Failure," Ph.D. Dissertation, School of Aerospace Engineering, Georgia Inst. of Technology, Atlanta, GA, March 1998.

[17]Laheru, K. L., "Development of a Generalized Failure Criterion for Viscoelastic Materials," *Journal of Propulsion and Power*, Vol. 8, No. 4, 1992, pp. 756–759.

A. M. Baz
Associate Editor